Materials Science and Engineering A, 555 (2012) 139-147

Powder metallurgical nanostructured medium carbon bainitic steel: kinetics, structure, and in-situ thermal stability studies

I. Lonardelli[*a,b], M. Bortolotti[c], W. van Beek [d], L. Girardini[e], M. Zadra[e], , HKDH Bhadeshia[a]

[a]University of Cambridge, Materials Science and Metallurgy, Pembroke Street, Cambridge CB2 3QZ, U.K.

[b]University of Trento, Materials Engineering and Industrial Technologies, Via Mesiano 77, 38123 Trento, Italy

[c]Fondazione Bruno Kessler, via Sommarive 18, 38123 Trento, Italy

[d]Swiss-Norwegian Beamlines, ESRF, BP 220, 38043 Grenoble Cedex, France

[e]K4-Sint, via Dante 300, 38057 Pergine Valsugana (TN), Italy

[*]**Corresponding author:** Ivan Lonardelli; e_mail: il244@cam.ac.uk. Tel: +44 (0) 1223 334336. Fax: +44 (0) 1223 334567.

Abstract

It has been possible to produce incredibly fine plates of bainitic ferrite separated by a percolating network of retained austenite in a medium carbon steel produced by mechanical alloying followed by spark plasma sintering and isothermal heat treatment. This is because the sintering process limits the growth of the austenite grains to such an extent that the martensite-start temperature is suppressed in spite of the medium carbon concentration. Furthermore, the fine austenite grain size accelerates the bainite transformation, which can therefore be suppressed to low

temperatures to obtain a nanostructure. Microscopy and *in situ* synchrotron X-ray diffraction were used to investigate the morphology and the thermal stability of the retained austenite during continuous heating. These latter experiments revealed a gradient of carbon concentration in the retained austenite and a reduced thermal stability in high carbon film-austenite. It was also possible to correlate the evolution of defect density and carbon depletion in both retained austenite and bainitic ferrite during tempering.

Keywords: Mechanical alloying, synchrotron X-ray diffraction, nanostructured bainite, kinetics, thermal stability.

Introduction

Carbide-free bainitic steels are representatives of a wide class of alloys in which interesting mechanical properties are obtained from relatively simple and cheap heat treatments. These treatments are intended to achieve a particular mixture of two-phases in which fine ferrite platelets alternate with thin films of retained austenite. The scale of this structure is such that contains a remarkably large density of interfaces, making it very strong even though there are no carbide particles present. Furthermore, the onset of plastic instability can be delayed by the presence of the austenite, which undergoes martensitic transformation during plastic deformation. The cheap way of introducing austenite into the microstructure is by preventing the precipitation of iron carbides during bainitic transformation. The carbon that is partitioned from bainitic ferrite then stabilizes the austenite. Silicon or aluminium are

commonly used to achieve this by affecting the chemical driving force for the precipitation of cementite from austenite [1]. The final phase mixture then consists of bainitic ferrite and retained austenite; when the transformation is conducted at a low homologous temperature, as done recently for high carbon low-alloy steels, slender platelets of bainitic ferrite (20-40 nm in thickness) are generated, embedded in a matrix of carbon-enriched austenite [2-4]. This particular structure, which is macroscopically isotropic, is strong (about 2000 MPa) and tough (30-45 MPa $m^{0.5}$). However, the isothermal heat treatment required to generate this structure is conducted at around 200^{o}C - 250°C, where transformation kinetics are slow and typically can take from 2 to 10 days to reach the desired degree of transformation. To reduce significantly the time accelerating the transformation kinetics, elements such as cobalt or aluminium must be added in order to enhance the free energy change accompanying transformation. Cobalt is unacceptable in situations where the steel will be irradiated [5], and large concentrations of aluminium make it difficult to process the liquid steel due to the blocking of nozzles [6]. An alternative approach is needed and the answer may lie in some recent work, which has reinforced the fact that the martensite-start temperature and the transformation rate of bainite are both correlated to the parent austenite grain size [7, 8]. Sintering is a mechanism by which exceptionally fine austenite grains can be ensured without thermomechanical processing and hence might represent a method of accelerating the transformation.
In the work presented in this paper, a nanostructured medium carbon bainitic steel was obtained by a combination of three steps: mechanical alloying, consolidation via spark plasma sintering and final heat treatment. The goal was to obtain a fine and stable microstructure before heat treatment in order to refine the austenite grain size due to austenitization and hence accelerate the subsequent bainitic transformation. *In*

situ high-energy synchrotron diffraction experiments were performed in order to study the thermal stability of the structure obtained.

Experimental procedure

A mixture of water atomized Astaloy CrL powder (1.5Cr and 0.24Mo wt%, with an average particle size of 75 μm), Ni elementary powder (2.7 wt%), FeSi powder as a source of silicon (1.89 wt%) and graphite as a source of carbon (0.5 wt%) was prepared by mixing in a Turbula apparatus for 15 min. The chemical composition measured after ball milling was Fe-0.48C-1.92Si-2.62Ni-1.47Cr-0.24Mo wt%. The alloy was designed on the basis of the theory [4,9] that predicts the highest temperature at which bainite (B_s) and martensite (M_s) can start to form in a steel of a given composition. These two temperatures constitute the upper and lower limits at which the isothermal heat treatment can be done to generate bainite. However, more refined microstructures are obtained by transforming at the lowest temperature while avoiding the martensitic transformation [10].

Mechanical alloying was carried out in a planetary ball mill Fritch Pulverisette 6 at 450 rpm for 4.5 h milling time. Cycles of 3 min on + 12 min off were used in order to avoid mill overheating. Before milling, the jar was sealed and kept under a low vacuum atmosphere.

The consolidation of the powder was made in a "SPS-1050" apparatus, Sumitomo Coal Mining Company Ltd.®. Small bars of the section of 10 × 5 mm and 50 mm length for dilatomeric study and dog-bone samples (5 × 5 mm section and 20 mm gauge length) for tensile tests were sintered in graphite dies. During SPS, the temperature increased up to 600°C with the pressure maintained at 6 MPa. Above

600°C, the heating rate was set at 100°C/min up to the maximum sintering temperature and the pressure was increased to 60 MPa in 2 min and maintained till the end of the soaking time.

The kinetics of the isothermal transformation was studied using a Bahr dilatometer (type 805 A/D).

Austempering heat treatment were performed at austenitising temperature of 1050°C with a selected soaking time of 30 minutes. A heating rate of 10°C/min was adopted to reach 1050°C. The process atmosphere was vacuum with an absolute pressure of 8×10^{-1} mbar at temperatures below 650°C. A back-fill atmosphere of 100 mbar Ar/H_2 mixture (90/10 vol%) was adopted for temperatures above 650°C. Samples were forced-cooled at 18°C/s using an 8 bar supply of nitrogen, to the isothermal transformation temperature (240°C). The soaking time selected was 4 h at 240°C in vacuum. The samples were characterized using optical microscopy, field emission - scanning electron microscopy (FE-SEM) with accelerating voltage of 15 kV and transmission electron microscopy (TEM). Preliminary investigations on the powder and on the consolidated samples before and after heat treatment, were performed using conventional X-ray measurements with a Cu Kα (λ=1.5418 Å) source and an image plate detector over the 2θ range from 30° to 90° in reflection geometry. Cylindrical samples of 1 mm diameter and 10 mm length were machined from the isothermally transformed material for the *in situ* continuous heating experiment. The experiment was carried out on the synchrotron facility at the Swiss-Norwegian Beam Line BM01, ESRF in Grenoble, France. During heating (5°C/min.) from RT to 650°C using a hot air blower, the sample was exposed to an X-ray beam of monochromatic wavelength λ=0.502467 Å and a beam size of 5 mm horizontal × 0.8 mm vertical. The temperature was monitored with a thermocouple in contact with the sample

during the entire experiment. A 2-circle diffractometer was available for high-resolution powder diffraction measurements. Each circle has a high precision encoder mounted directly on the rotation axis. The experiment was performed in transmission geometry with an illuminated volume two orders of magnitude higher compared to a normal X-ray experiment in reflection. The detector has 6 fast counting chains so that 6 patterns can be collected simultaneously, with an offset of $2\theta = 1.1°$, in order to reduce the total data collection time to a minimum.

Diffraction spectra collected every 25°C interval during heating at 5°C/min, between room temperature to 650°C, were entered into the program MAUD (Materials Analysis Using Diffraction) [11], and fit using the Rietveld procedure [12]. A reference specimen of Si powder standard (NIST SRM-640c) was used to determine the wavelength of the incident beam (0.502466 Å) and calibrate the instrument parameters for the integrations.

The fractions of retained austenite and bainitic ferrite as well as the lattice parameters were evaluated using the 111, 200 austenite peaks and 110, 002 ferrite peaks. Line profile analysis was performed using Popa approach [13] incorporated into the Rietveld algorithm to account crystallite size and microstrain ($\langle e^2 \rangle^{1/2}$) this latter quantity being proportional to the square root of dislocation density.

The austenite and ferrite carbon content was estimated according to relationships published the literature [14, 15]:

$$a_\gamma = 3.5780 + 0.033w_C - 0.0002w_{Ni} + 0.0006w_{Cr} + 0.0031w_{Mo} \quad (1)$$

where a_g is the lattice parameter of austenite in Å, and w_i is the concentration of element i in wt%. For ferrite we can write

$$a_{\alpha} = 2.8664 + \frac{(a_{Fe} - 0.279x_C)^2(a_{Fe} + 2.496x_C) - a_{Fe}^3}{3a_{Fe}^2} - 0.03x_{Si} + 0.07x_{Ni} + 0.31x_{Mo} + 0.05x_{Cr} \quad (2)$$

where x_i is the concentration in mole fraction and a_F is the lattice parameter of ferrite in Å of pure iron.

Results and discussion

Characteristics of the as milled powder

Fig. 1a and b show the morphology of the milled powder after 4.5 h of milling at 450 rotations per minute (rpm). The energetic ball milling strongly reduces the powder particle size. The XRD results revealed a ferritic microstructure with no peaks referred to the single elements and an average crystallite size of 25 nm. Some additional consideration about the evolution of the oxygen content during mechanical milling must be discussed. The oxygen content of the powder blended before ball milling can be estimated in the range of 0.14 – 0.16 wt%, according to the chemical analysis provided by Hoganas. The ball milling was performed in a low vacuum atmosphere and the free volume in the jar is limited. For this reason only a small quantity of oxygen contamination can be expected during mechanical alloying. As already mentioned, ball-milling process strongly reduces the powder particle size (from an average of 75 μm to 9.1±2.1μm), with an obvious increase of the particles surface. When the processed powder is exposed to the atmosphere, the passivation process occurs and the oxygen measured was 0.23 wt%.

Density and microstructure of the sintered material

The spark plasma sintering (SPS) system is a method for full density sintering of ball-milled metal powder. In spite of the high oxygen content and the low compressibility at room temperature due to the high powder microhardness, full density conditions can be reached [16-19]. This is an important point when processing the metal powder having in mind target of high mechanical properties.

Fig. 2a shows the SPS densification curves of the material up to 1000°C. The displacement rate curve is characterized by two distinct phenomena: first, the increase of the rate above 550°C that corresponds to an increasing of applied pressure, is due to the rearrangements of the powder particles. A second event with a peak at 700°C, is ascribed to the densification occurring when the resistant to the plastic deformation of the material decreases as a consequences of the thermal softening [19]. The densification rate decreases to zero at 820°C. Between 600°C and 800°C, the pressure increases from 6 MPa to 60 MPa.

SPS experiments were carried out at 950°C, 1000°C and 1050°C and the hardness as well as the relative density measured after sintering are displayed in Fig. 2b. Both, the hardness measurements and the relative density estimated with the Archimedes method show that the full density is reached at 1000°C, with a soaking time of 3 min. Even after sintering at 950°C for 1 min, the steel has a low degree of porosity, reaching 99.1% of the relative density.

Light optical microscopy (LOM) and high resolution X-ray from synchrotron revealed that after sintering the microstructure is mainly martensitic with 9% of retained austenite (Fig. 3a and b). Within the limit of LOM, no residual significant porosity is observed and no carbides were detected. However, the small black dots in Fig. 3a can be ascribed to a homogeneous distribution of very fine oxide particles.

The oxygen measured on the milled powder before sintering, cannot be reduced by means of the standard carbon/oxide chemical reactions [20, 21]. This aspect is also confirmed from the quantitative analysis of the carbon and oxygen performed after SPS on the bulk samples where identical vales were found [22]. The thermodynamic conditions in terms of temperature and process atmosphere are satisfied but the oxide reduction can result in open porosity. The chemical reaction involving the reduction of oxides cannot evolve without a route for the reduction products to escape.
We can argue that SPS is a reliable method to realize full density sintered bulk components but the oxygen eventually present in the powder cannot be reduced.

Heat treatment, microstructure and mechanical properties

After sintering the steel was studied in order to investigate the martensite-start temperature and the kinetics of the bainitic transformation. After austenitization at 1050°C for 30 min and a cooling rate to RT of 15°C/s, Ms was experimentally estimated, using dilatometry to be 215°C, about 50°C below the calculated value using thermodynamic and kinetics models developed to calculate isothermal transformations diagrams [23, 24] that account only the steel chemical composition (Fig. 4a). Another important feature observed in the dilatometer during isothermal heat treatment is that the time required to initiate the transformation at 240°C is around 1200 s, significantly small compared with that expected for similar compositions at the same temperature for a steel produced by conventional technology (Fig. 4b).
This discrepancy can be explained if we consider that the time to achieve the desired microstructure depends on several factors. The chemical composition and the transformation temperature can significantly alter the kinetics of the bainite

transformation. Another important variable is the grain size of the starting austenite. Figs 5a and b show the prior austenite grain size obtained after austenitization at 1050°C for 30 min and a subsequent rapid cooling (20°C/s) to 650°C followed by an holding of 2 min and final cooling to RT to induce pearlitic transformation at the grain boundary. The average grain size is 8.0±2.9 μm and the reduction of the Ms temperature is in good agreement with a recent work in which the dependence of Ms with the prior austenite grain size is well documented [7]. The reduced time to initiate the transformation may be explained in terms of the austenite grain boundary surface per unit volume, which inevitably contributes to the nucleation of bainite. Fig 5c and 5d show the optical micrographs after 40 min and 4 h at 240°C respectively. X-ray diffraction from synchrotron revealed that the volume fraction of retained austenite after the isothermal heat treatment is 0.225±0.008. The microstructure obtained is fairly homogeneous and consists of bainitic ferrite sheaves and retained austenite, the latter in the form of films constituting an interconnected network since the fraction of austenite is beyond the percolation threshold [4]. Only a minority part of retained austenite can be identified to be in the form of blocks with an average size of about 1 μm or less. Figs 6a, b and c show SEM micrographs at different magnifications after polishing and etching with nital (2%). The austenite network varies in terms of the film austenite thickness and also the carbon concentration is expected to increase with the decreasing of the film thickness [25]. Any gradients in the carbon concentration of the retained austenite would explain the strong peak asymmetry observed in the high resolved diffraction pattern (Fig. 6d). Our previous work dealt with the decomposition of retained austenite in bainitic steel obtained by transformation at 380°C, with a microstructure that had a much greater quantity, in excess of 50%, of block, low-carbon austenite, and film austenite with a

thickness around 100 nm. In that case the diffraction pattern showed two distinct components [26]. Fig. 6d from the present work shows the 111 austenite peak with a strong asymmetry describing mainly a carbon concentration gradient in the retained austenite network. This particular peak shape can be considered as the superposition of the several peaks with different lattice parameters and different peak breadths consistent with a film thickness network in the range of 15 to 100 nm (Fig.6c). However, the experimental austenite peak profile can be, in first approximation, deconvoluted in two superimposed peaks, one accounting the high carbon film-austenite and a second to the coarser low-carbon.

Some spherical oxides are visible between and within the platelets (Fig. 6b). These oxides which are formed during SPS consolidation process and also during subsequent heat treatment at 1050°C are thought to play a key role by keeping the grain size stable via Zener pinning.

Without the oxide particles the grains should undergo rapid grain growth during the heating of consolidation or during the heat treatment. In this sense the oxide particles play an important role in maintain a fine-grained bulk matrix even after exposure at elevated temperatures.

The tensile behaviour is characterised by a 0.2% proof strength of 1320 MPa combined with a uniform deformation up to fracture at 1860 MPa (Fig. 7a). The main feature is the total elongation of about 7% and an excellent strain hardenability provided by the network of fine retained austenite. This high strain hardening and uniform elongation can be attributed to the stress or strain induced martensitic transformation of the retained austenite [27]. However, as recently reported for medium carbon bainitic steels [28] the morphology of the retained austenite is an important factor that has to be considered in the mechanical stability of the γ austenite

during strain. Fig. 7b shows the incremental strain hardening as a function of true plastic strain. The straight line corresponds to the instability criterion $e_p=n$ where e_p is the true plastic strain and n is the incremental strain hardening exponent. The high strain hardening capacity is maintained up to 3% of plastic strain. As the true strain increases, the strain hardening tends to decrease rather rapidly. X-ray investigations on the deformed sample after tensile testing to fracture, reveals that the volume fraction of retained austenite content is reduced to 0.11±0.01 measured at about 1 mm from the fracture surface (transversal section). This value is in good agreement with recent work in which formation of deformation-induced martensite, fundamental to the achievement of ductility, can only be tolerated if the austenite maintains a uniform and percolated structures [29].

The fracture surface illustrated in Fig. 8a-d shows a totally ductile behaviour with no indication of cleavage, and confirms the presence of spherical silica nanoparticles. The ductile behaviour is the result of the particular microstructure in which the film austenite forms an interconnected network between bainitic ferrite sheaves (Fig 9a). However, high magnification SEM reveals that tiny silica particles appear distributed uniformly in the matrix (Fig. 9b). It should be pointed out that the starting water-atomized Fe-Cr powder had 0.14 wt% of oxygen and after mechanical alloying the quantity measured was 0.23%. A consistent improvement in terms of uniform elongation is expected by using a starting atomized powder with less oxygen.

Thermal stability of the microstructure

Fig. 10 shows the experimental 2D plot that covering a broad range of diffracted Bragg angles during in-situ heating of the isothermally generated mixture of fine bainite and retained austenite, up to 650°C from room temperature, with a heating rate

of 5°/min. White arrows indicate clearly the cementite peaks that start to be detectable at 450°C. Note the changes in the position of the {111} and {200} austenite peaks at 400-450°C, with a sensible reduction of the lattice parameter up to 600°C. As already mentioned, the residual austenite peaks are affected by a strong asymmetry due to the gradient of the carbon content in the retained austenite network. The volume fraction of the blocky austenite is small and the thickness of the film austenite network varies between 15 and 100 nm (Fig. 6c and 9a) with a consequent broad distribution of the carbon content as measured in a recent work by using atom probe tomography [25]. The changes in quantities of both the high carbon and low carbon austenite as well as the lattice parameters during the heating experiment are reported in Figs. 11 and 12. The lattice parameter changes due to the thermal expansion was calculated using the following equation:

$$a^T = a^{298}[1 + e(T - 298)] \quad (3)$$

where T is the temperature in K, and a is the lattice parameter of austenite and ferrite. The thermal expansion coefficient for austenite and ferrite considered was e_g=2.065 × 10^{-5} K^{-1} and e_a=1.244 × 10^{-5} K^{-1} respectively [30].

From a quantitative point of view (Fig. 11 a), the austenite starts to decompose above 450°C, with cementite that starts to grow from the carbon enriched austenite. This assumption is supported by the evolution of diffraction pattern during heating (Fig. 11 b), where the changes in peak shape and peak position of 111 austenite are clearly recognized. However, the change in lattice parameter of the high carbon enriched austenite is above 400°C (Fig. 12 a) and between 400°C and 450°C there is a sort of incubation period in which the carbides are not detectable and no decomposition of

retained austenite is observed. The super-saturated ferrite lattice start to deviate from the linear thermal expansion between 400°C and 425°C. Above 450°C up to 525°C relevant structural changes are detected from the lattice parameter as well as from the quantitative analysis. Particularly, the decomposition takes place only in a small amount of retained austenite network and the residual austenite has a significantly smaller carbon content. This can be quantitatively observed as a decrease in the high-carbon retained austenite but surprisingly, although the overall quantity of austenite decreases (Fig. 11a), there is an increase in percent of the austenite with less carbon at temperatures close to 500°C. This must be due to a redistribution of carbon through homogenisation, rather than the growth of austenite, which is not possible from a thermodynamic point of view [31]. At 525°C, about 0.2±0.008 of the volume fraction of retained austenite survives, but decomposition then proceeds with a noticeably increasing rate due to cementite formation. Above 600°C, the synchrotron X-ray determined retained volume fraction of austenite is 0.152±0.006. The calculated carbon content of bainitic ferrite and retained austenite during continuous heating is reported in Fig. 12b. The loss of carbon in austenite and supersaturated ferrite is clearly evident. Particularly, the amount of carbon in supersaturated ferrite appears to decrease substantially during tempering above 400°C, in contrast to a recent work in which the carbon in a superbainitic steel, was measured with atom probe tomography where the amount of material that can be examined is much more limited [25].
After formation of superbainitic microstructure, for the retained austenite becomes impossible to accommodate all the carbon that is rejected from the ferrite [32], and the enrichment in carbon of retained austenite is first controlled by diffusion in ferrite, but is later driven by diffusion in austenite [33]. During continuous heating, no further enrichment of carbon from supersaturated ferrite into austenite was observed.

However, some considerations in terms of microstructural changes must be discussed. Fig 13a shows the average microstrain changes with the temperature. In general, the annihilation of crystal defects can be detected by a decrease of the microstrain. In both retained austenite and supersaturated ferrite, the decrease of the defect density is concomitant with the loss of carbon and the formation of cementite that becomes quantitatively detectable at 450°C (black filled circles Fig. 11a). At 400°C a significant decrease of microstrain in supersaturated ferrite and, in high carbon enriched austenite can be explained as a dislocation annihilation. If the dislocation density decreases with increasing temperature, the carbon might be rejected from the bainitic ferrite and film austenite. Moreover, the kinetics of reaction in small austenite is much more stimulated due to the large surface to volume ratio of any nano-sized particles of austenite. Fluctuations of carbon concentration detected in supersaturated ferrite were attributed to the presence of high-density defects regions in which high level of carbon can be trapped at dislocations and nanotwins [34-36]. Carbon at defects has a lower energy than cementite, so cementite precipitation occurs when defects are annealed. This interpretation is consistent with our observations in which cementite is seen around 450°C (Fig. 11a) after recovery of microstrain (Fig. 13a). The ability of dislocations to trap the carbon atoms was originally suggested by Kalish and Cohen [37]. Recently, the carbon level of the Cottrell atmosphere in the vicinity of the dislocation were estimated to be 7.4 at.% [38] in agreement with a previous work in which Wilde *et al.* [39] observed a maximum carbon concentration within a dislocation atmosphere of 8 at.%. The relationship between defect density and carbon content in bainitic ferrite was also investigated by using laboratory X-ray diffraction [40]. Our experimental observations suggest that as reported in Fig. 13b, there is a correlation between dislocation recovery and changes of carbon in retained

austenite as well as in bainitic ferrite during tempering. Between 400°C and 450°C a significant decrease of defect density occurs with a subsequent decreasing (450°C-500°C) in carbon content. This correlation is particularly significant in high carbon film austenite in which the size of the grains is well below 100 nm. At this level of size the full and partial dislocations originated during low temperature bainitic transformation will annihilate at the grain boundary during tempering.

Summary

A high strength nanostructured bainitic steel has been produced by a powder metallurgy approach in which mechanically alloyed powder was spark plasma sintered to almost full density. Because of the oxygen (oxide) content of the resulting material, a very fine austenite grain size (8 μm) was obtained in spite of the necessary elevated temperature heat treatments. This resulted in a suppression of the martensite-start temperature, thus allowing isothermal transformation to bainite at the low homologous temperatures need to produce a nanostructured formation of plates, in spite of the fact that the alloy contained only 0.48 wt% carbon which compares with the 0.8-1 wt% typical in previous work on bulk nanostructured bainite. Furthermore, the fine parent structure also usefully accelerated the kinetics of the bainite reaction. This method was used to investigate the low temperature bainitic transformation in a context of medium carbon steel and a reduced starting austenite grain size.

In situ tempering experiments using synchrotron X-rays have confirmed that the high carbon austenite films are less stable than the austenite that contains less carbon. The experimental results suggest that within the limits of experimental error, there is no formation of e-carbide precursors prior to the onset of cementite precipitation. The driving force for the cementite precipitation is much higher in high carbon film

austenite. Dislocations and nanotwins can accommodate large quantities of carbon and the high level of microstrain calculated from the high carbon film austenite and bainitic ferrite peaks suggest a correlation between defect density and carbon concentration. Particularly, the size of the film austenite might play a key role in the mechanism of the recovery of dislocations. Partial and full dislocations in the context of grains below 100 nm are greatly influenced by the close proximity of the boundaries.

Acknowledgement

The authors are grateful to Prof. C. Migliaresi for the access to the Research Center BIOtech (Trento) for the high-resolution SEM micrographs. This work was partially supported by the European Union, Marie Curie Actions, Marie-Curie 7th Framework Programme, the Trentino programme research. We appreciate access to the synchrotron beam line BM01 at ESRF.

References

[1] E. Kozeschnik, H.K.D.H. Bhadeshia, Mat. Sci. Technol. 24 (2008) 343-347.

[2] F.G. Caballero, H.K.D.H. Bhadeshia, K.J.A. Mawella, D.G. Jones, P. Brown, Mat. Sci. Technol. 18 (2002) 279-284.

[3] F.G. Caballero, H.K.D.H. Bhadeshia, Current Opinion in Solid State and Materials Science 8 (2004) 251-257.

[4] H.K.D.H. Bhadeshia, Proc. Royal Soc. A, 466 (2010) 3-18.

[5] R. L. Kleuh, E. T. Cheng, M. L. Grossbeck, E. E. Bloom, Journal of Nuclear Materials, 280 (2000) 353-359.

[6] G. C. Duderstadt, R. K. Iyengar, J. M. Matesa, Journal of Metals 20 (1968) 89-94.

[7] H.S. Yang, H.K.D.H. Bhadeshia, Scripta Mater. 60 (2009) 493-495.

[8] S.J. Lee, J.S. Park, Y.K. Lee, Scripta Mater. 59 (2008) 87-90.

[9] H.K.D.H. Bhadeshia, Acta Metall. 29 (1981) 1117-1130.

[10] S.B. Singh, H.K.D.H. Bhadeshia, Mater. Sci. Eng. A A245 (1998) 72-79.

[11] L. Lutterotti, S. Matthies, H.R. Wenk, A.S. Shultz, J.W. Richardson, J. Appl. Phys. 81 (1997) 594-600.

[12] H.M. Rietveld, J. Appl. Cryst. 2 (1969) 65-71.

[13] N.C. Popa, J. Appl. Cryst. 31 (1998) 176-180.

[14] H.K.D.H. Bhadeshia, S.A. David, J.M. Vitek, RW Reed, Mater. Sci. Technol. 7 (1991) 686-698.

[15] D.J. Dyson, B. Holmes, J. Iron Steel Inst. 208 (1970) 469-474.

[16] Y. Minamino, Y. Koizumi, N. Tsuji, N. Hirohata, K. Mizuuchi, Y. Ohkanda, Sci. Technol. Adv. Mater. 5(1-2) (2004) 133-143.

[17] C. Menapace, I. Lonardelli, M. Tait, A. Molinari, Mat. Sci. Eng. A 517 (2009) 1-7.

[18] H.W. Zhang, R. Gopalan, T. Mukai, K. Hono, Scripta Mater. 53 (2005) 863-868.

[19] S. Libardi, M. Zadra, F. Casari, A. Molinari, Mater. Sci. Eng. A 478 (1-2) (2008) 243-250.

[20] S. Takaki, K. Kawasaki, Y. Kimura, J. Mater. Process. Tech. 117 (2001) 359-363.

[21] P. Ortiz, F. Castro, Powder Metall. 47 (2004) 291-298.

[22] L. Girardini, I. Lonardelli, High strength Steel through mechanical alloying and advanced vacuum heat treatments. Proceedings of International Super High Strength Steel Congress-Peschiera del Garda-Italy-17-20 October 2010 (CD-ROM).

[23] Materials Algorithms Project (MAP), Department of Materials Science and Metallurgy, University of Cambridge, UK. http://www.msm.cam.ac.uk/map.

[24] H.K.D.H. Bhadeshia. A thermodynamic analysis of isothermal transformation diagrams Met. Sci. 16 (1982)159-65.

[25] F.G. Caballero, M.K. Miller, A.J. Clarke, C. Garcia-Mateo, Scripta Mater. 63 (2010) 442-445.

[26] A.S. Podder, I. Lonardelli, A. Molinari, H.K.D.H. Bhadeshia, 2011 Proc. Royal Society A 467 (2011) 3141-3156.

[27] L. Samek, E. de Moor, J. Penning, B.C. De Cooman, Metall. Mater. Trans. A, 2006, vol. 37A, pp. 109 – 24.

[28] F.G. Caballero, C. Garcia-Mateo, J. Chao, M.J. Santofimia, C. Capdevila, C.G. de Andrés, ISIJ International 48 (2008) 1256-1262.

[29] H.K.D.H. Bhadeshia, Ironmaking Steelmaking 34 (2007) 194-199.

[30] M. Takahashi, Reaustenitization from bainite in steel,Ph.D.thesis, University of Cambridge, http://www.msm.cam.ac.uk/phase-trans/2000/phd.html#Takahashi.

[31] J. R. Yang, H. K. D. H. Bhadeshia, Mater. Sci. Eng. A A131 (1991) 99-113.

[32] S.A. Mujahid, H.K.D.H. Bhadeshia, Acta Metall. Mater. 40 (1992) 389-396.

[33] M. Hillert, L. Hoglund, J. Agren, Acta Metall. Mater. 41 (1993) 1951-1957.

[34] H.K.D.H. Bhadeshia, A.R. Waugh, Acta Metall. 30 (1982) 775-784.

[35] A.J. Clarke, J.G. Speer, M.K. Miller, R.E. Hackenberg, D.V. Edmonds, D.K. Matlock, F.C. Rizzo, K.D. Clarke, E. De Moor, Acta Mater. 56 (2008) 16-22.

[36] F.C. Caballero, H.-W. Yen, M.K. Miller, J.-R. Yang, J. Cornide, C. Garcia-Mateo, Acta Materialia, 59 (2011) 6117-6123.

[37] D. Kalish, M. Cohen, Mater Sci Eng 6 (1970) 156-166.

[38] F.G. Caballero, M.K. Miller, S.S. Babu, C. Garcia-Mateo, Acta Mater. 55 (2007) 381-390.

[39] J. Wilde, A. Cerezo, G.D.W. Smith, Scripta Mater. 43 (2000) 39-48.

[40] C. Garcia-Mateo, M. Peet, F.G. Caballero, H.K.D.H. Bhadeshia, Mat. Sci. Technol. 20 (2004) 814-818.

Figures

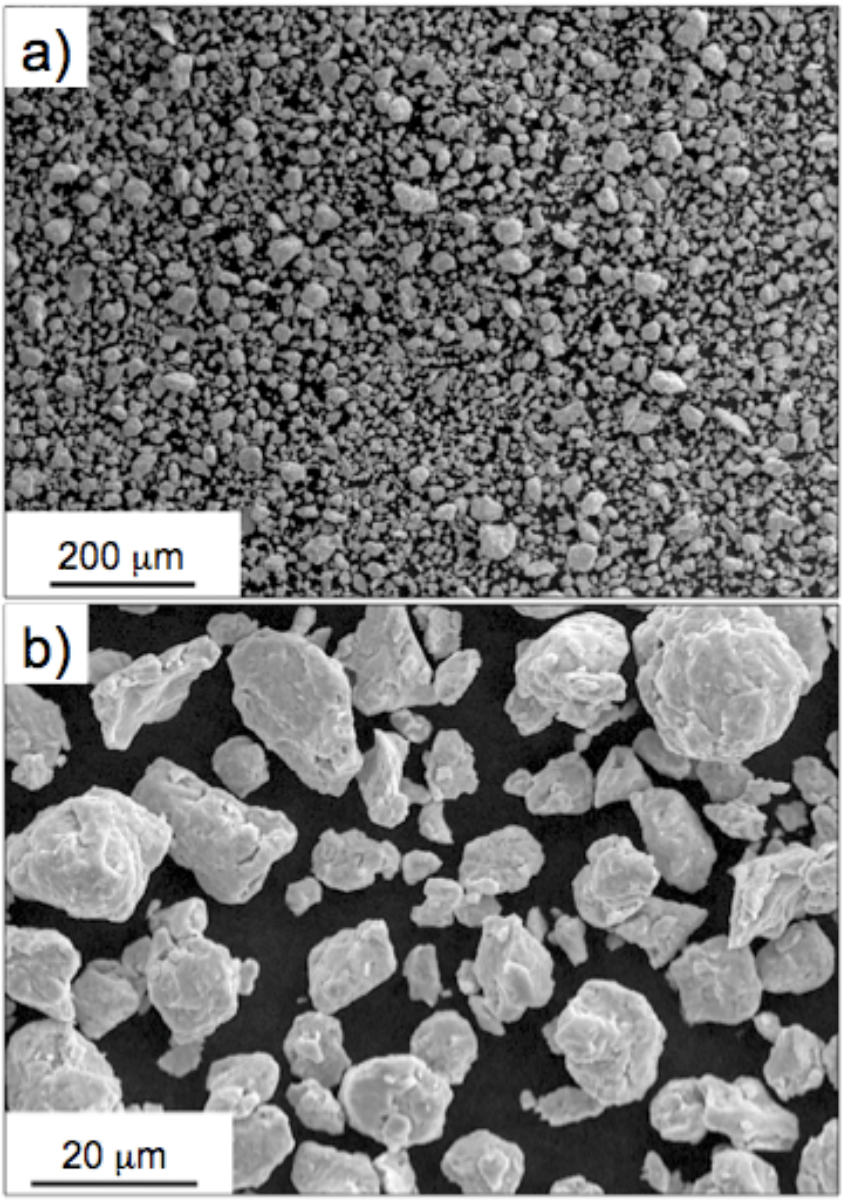

Fig.1. SEM micrographs of the milled powder after 4.5 h at 450 rpm. The mean particle size is 9.1±2.1 μm

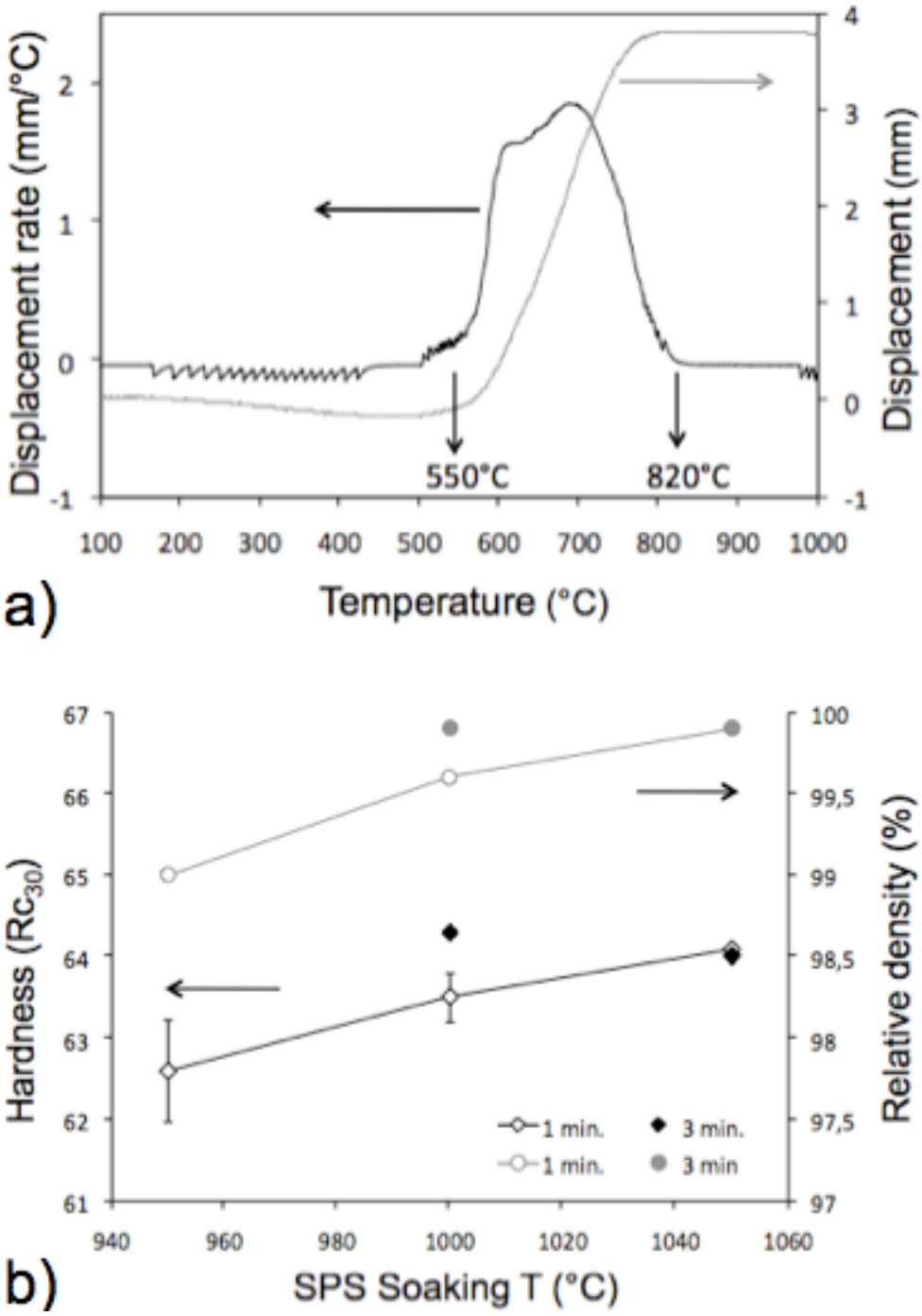

Fig.2. Spark plasma sintering (SPS) curve of the milled powder (a). Gray line represents the punch displacement and black line the displacement rate. Density and microhardness of the sintered materials at different SPS soaking temperature and time are reported (b).

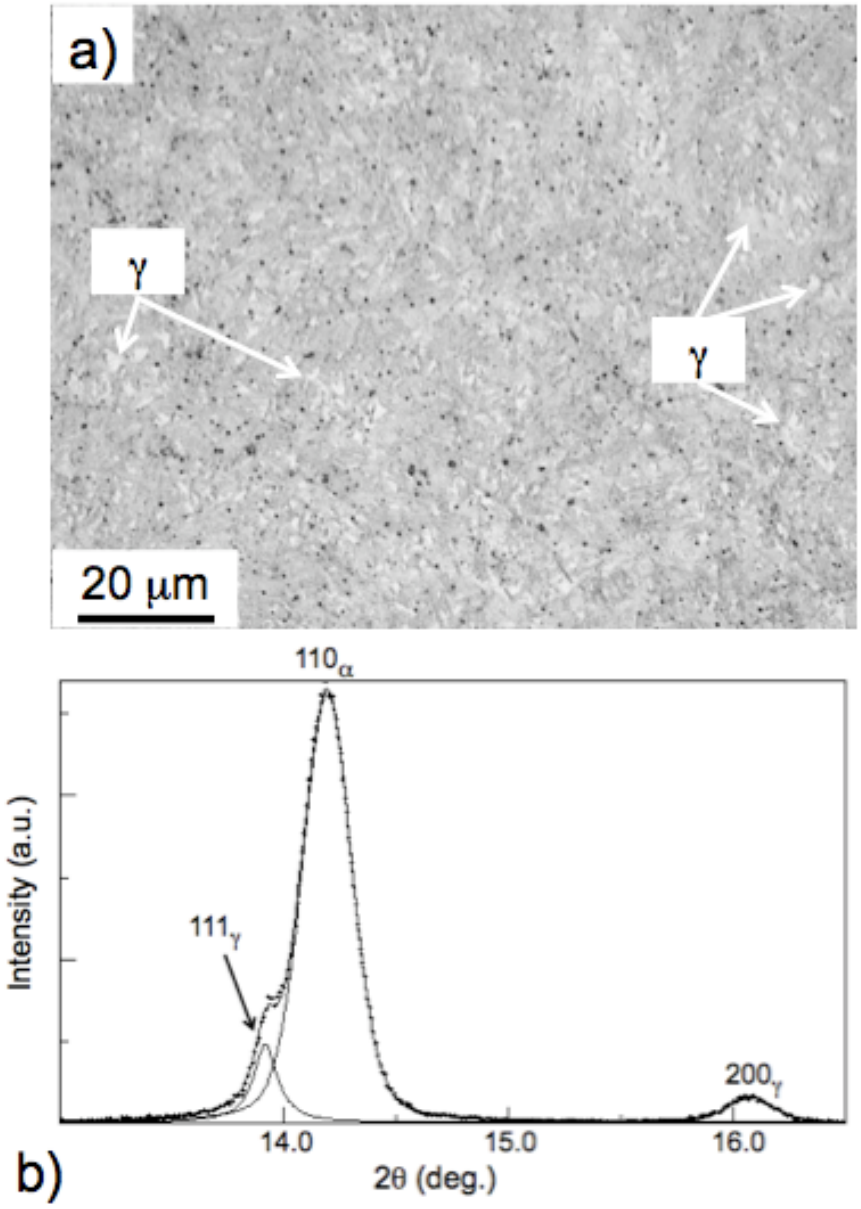

Fig.3. Optical micrograph of the SPS sintered material (1000°C for 3 min) (a) and, X-ray diffraction pattern (b) show the microstructure and the quantitative analysis respectively. The microstructure is mainly martensitic with 9% of retained austenite at RT.

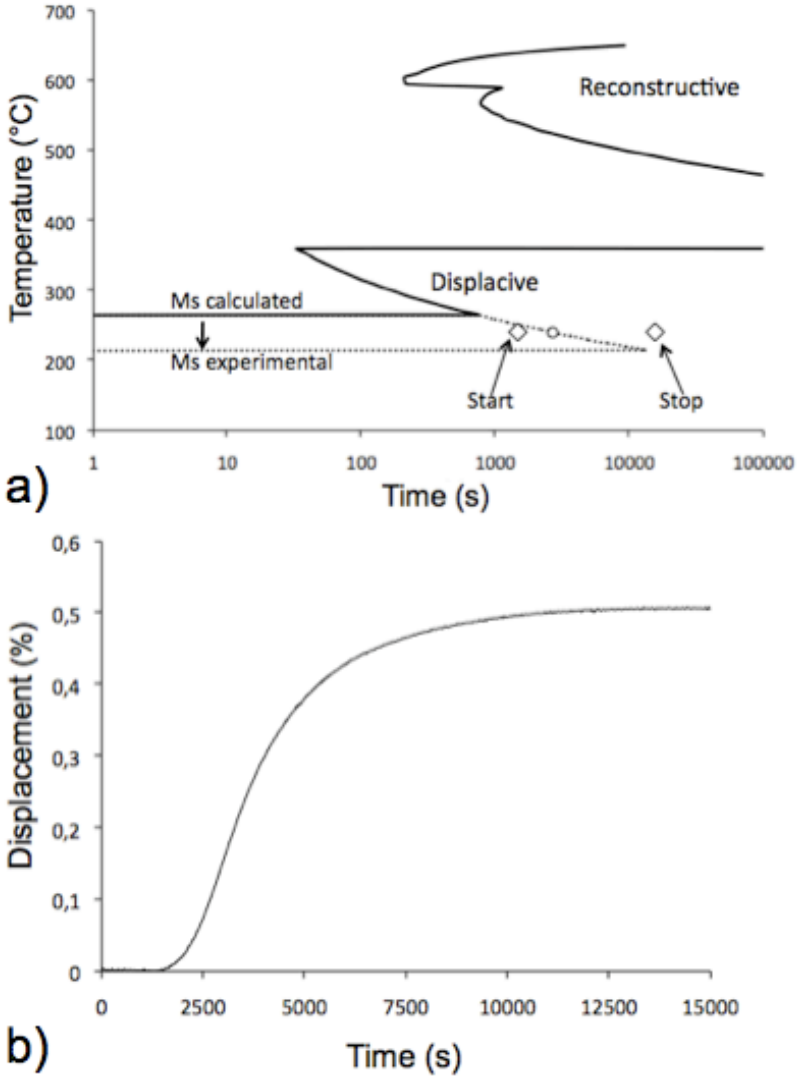

Fig.4. Calculated TTT diagram of the designed steel (a). Experimental dilatometric curve collected during isothermal holding at 240°C (b) describes the kinetics of the bainitic transformation. The time required to initiate and finish the transformation is compared to the calculated one (a).

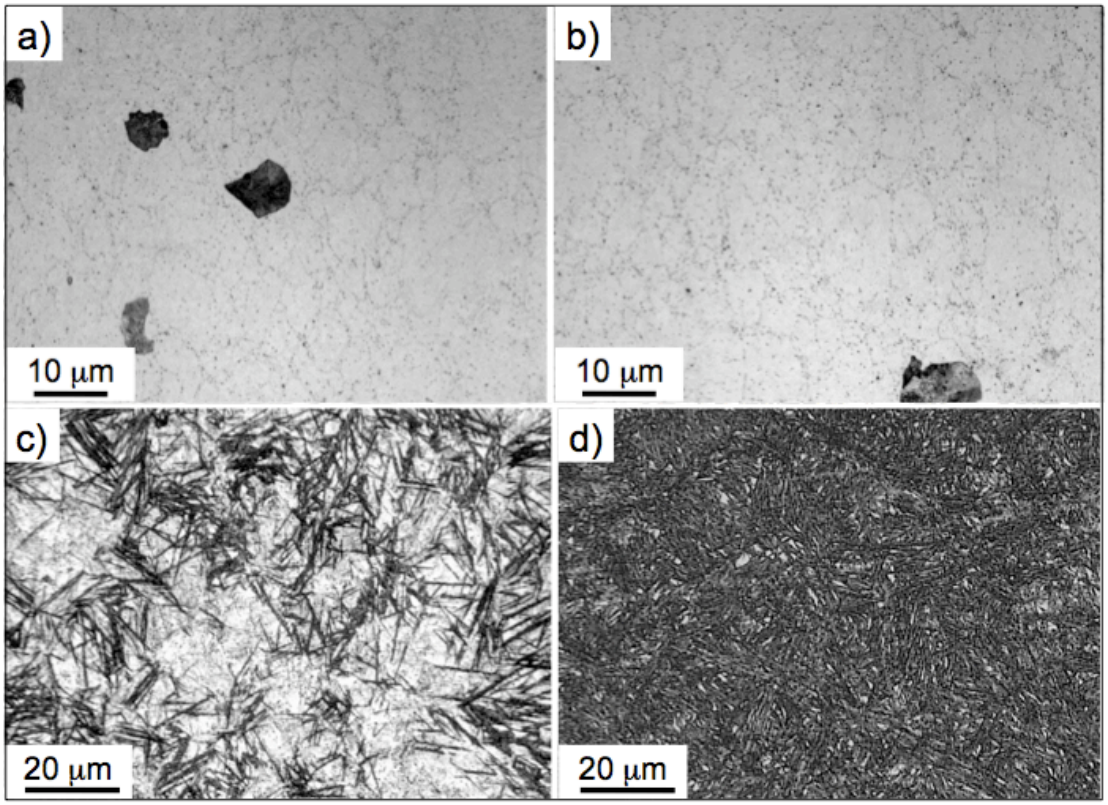

Fig.5. Optical micrographs of the sample after austenitization at 1050°C for 30 min and rapid cooling (20°C/sec) at 650°C followed by a holding of 2 min and final cooling to RT. The grain boundary of parent austenite and some perlitic grains are well recognized. The microstructure after 40 min and 4 h of holding at 240°C is documented in (c) and (d) respectively.

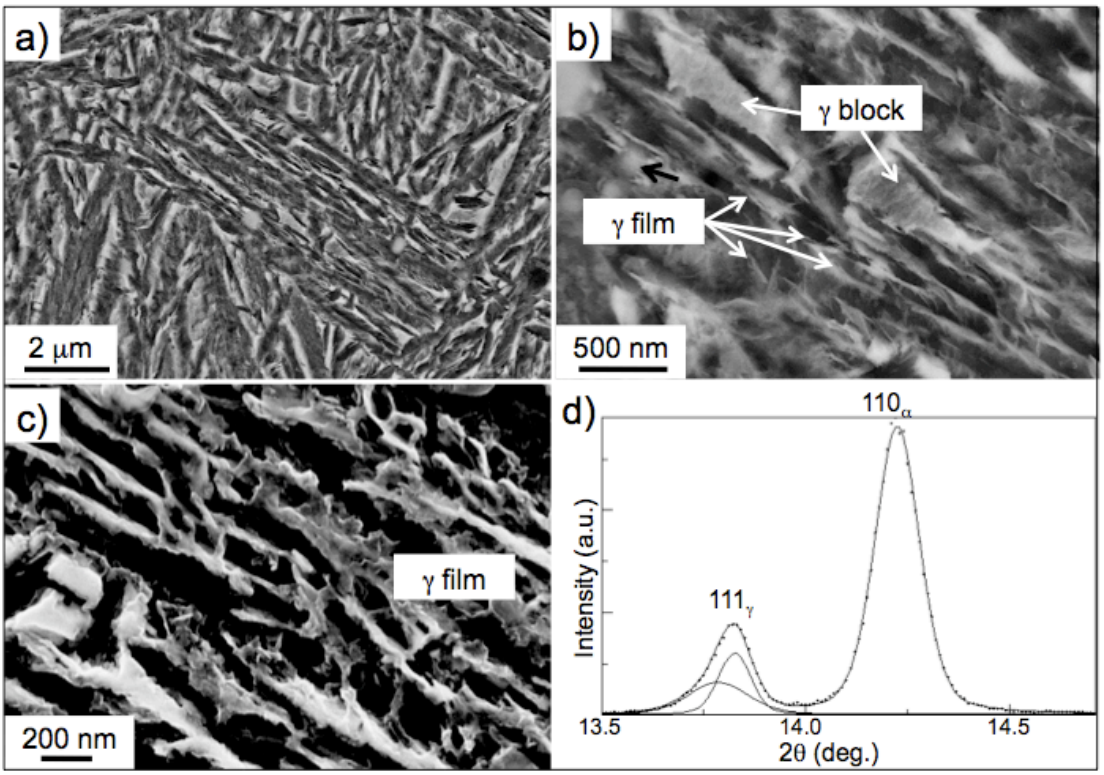

Fig.6. SEM micrographs at different magnifications show the microstructure obtained after isothermal heat treatment at 240°C for 4 h. The retained austenite network thickness (c) ranges between 10 to 100 nm. Some blocky austenite below 1 micron can be also recognized (a, b). X-ray diffraction pattern is shown in (d).

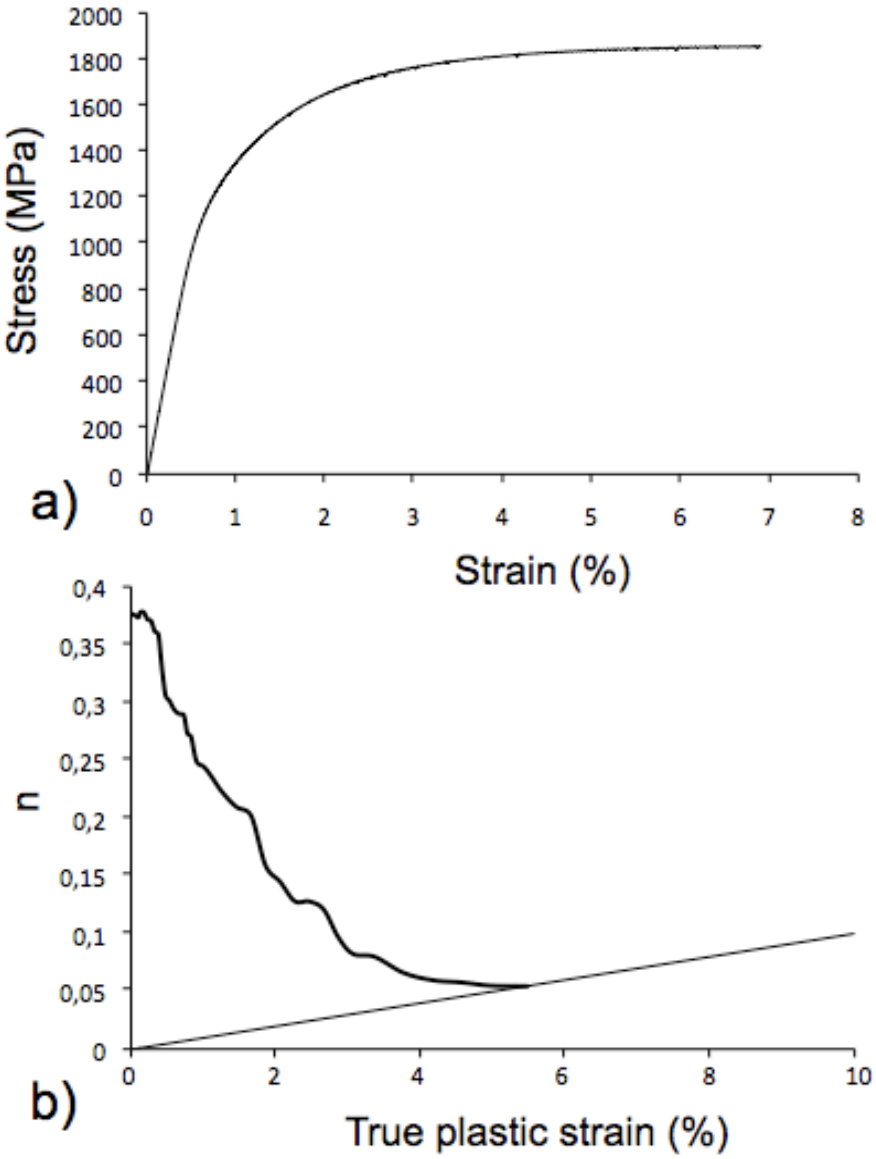

Fig.7. Tensile stress-strain curve (a) and incremental strain hardening as a function of true plastic strain (b).

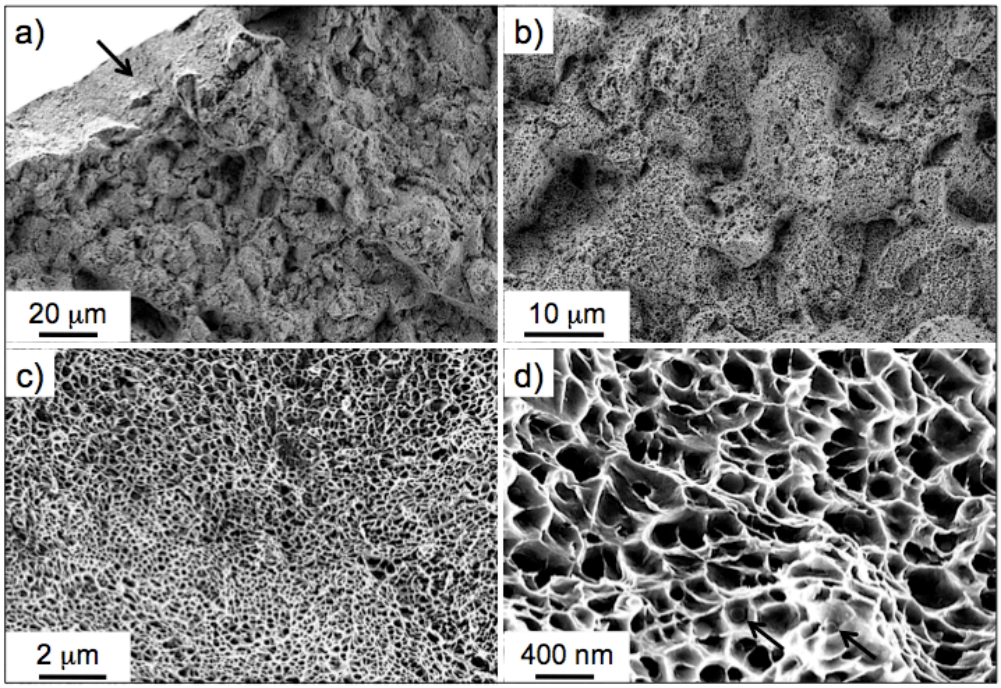

Fig. 8. SEM micrographs show fracture surface at different magnification levels. Arrow in (a) is pointed on the crack initiation that is located on the surface of the sample. Two arrows in (d) show the spherical silica particles inside of nano-dimples.

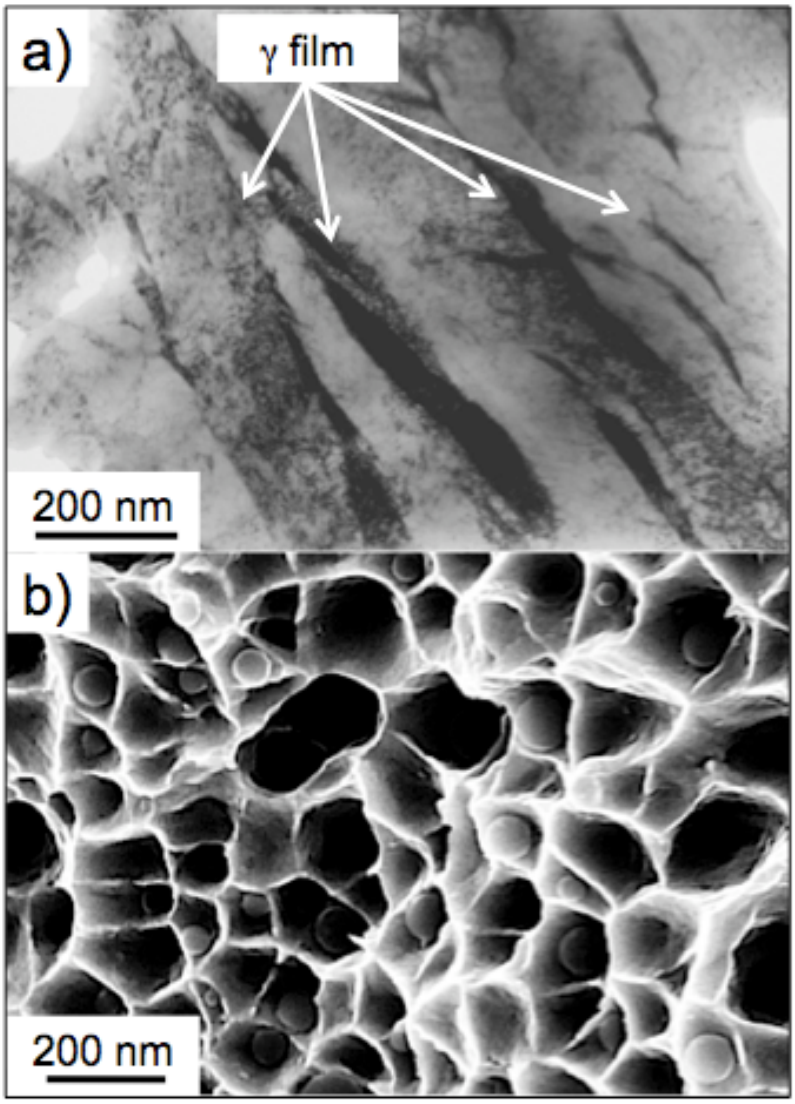

Fig.9. TEM micrograph (a) shows the film austenite between bainitic ferrite sheaves. High magnification SEM micrograph (b) shows the spherical silica particles with the size that ranges between 30 and 80 nm.

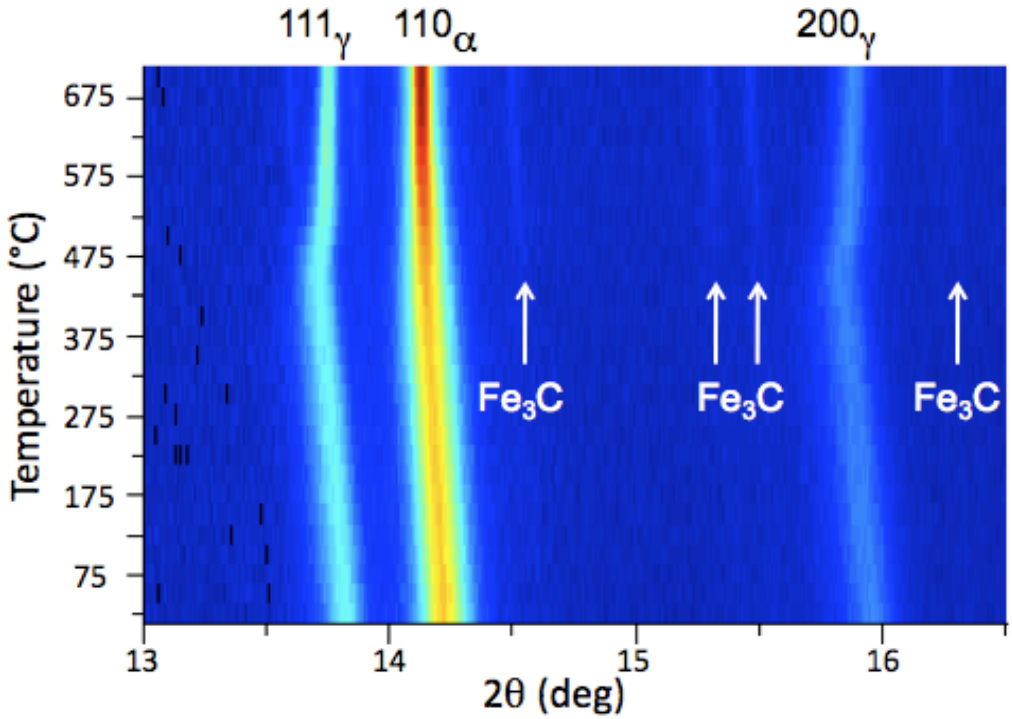

Fig.10. Experimental 2D plot shows the qualitative evolution of retained austenite, bainitic ferrite and cementite during continuous heating using in situ X-ray synchrotron diffraction technique.

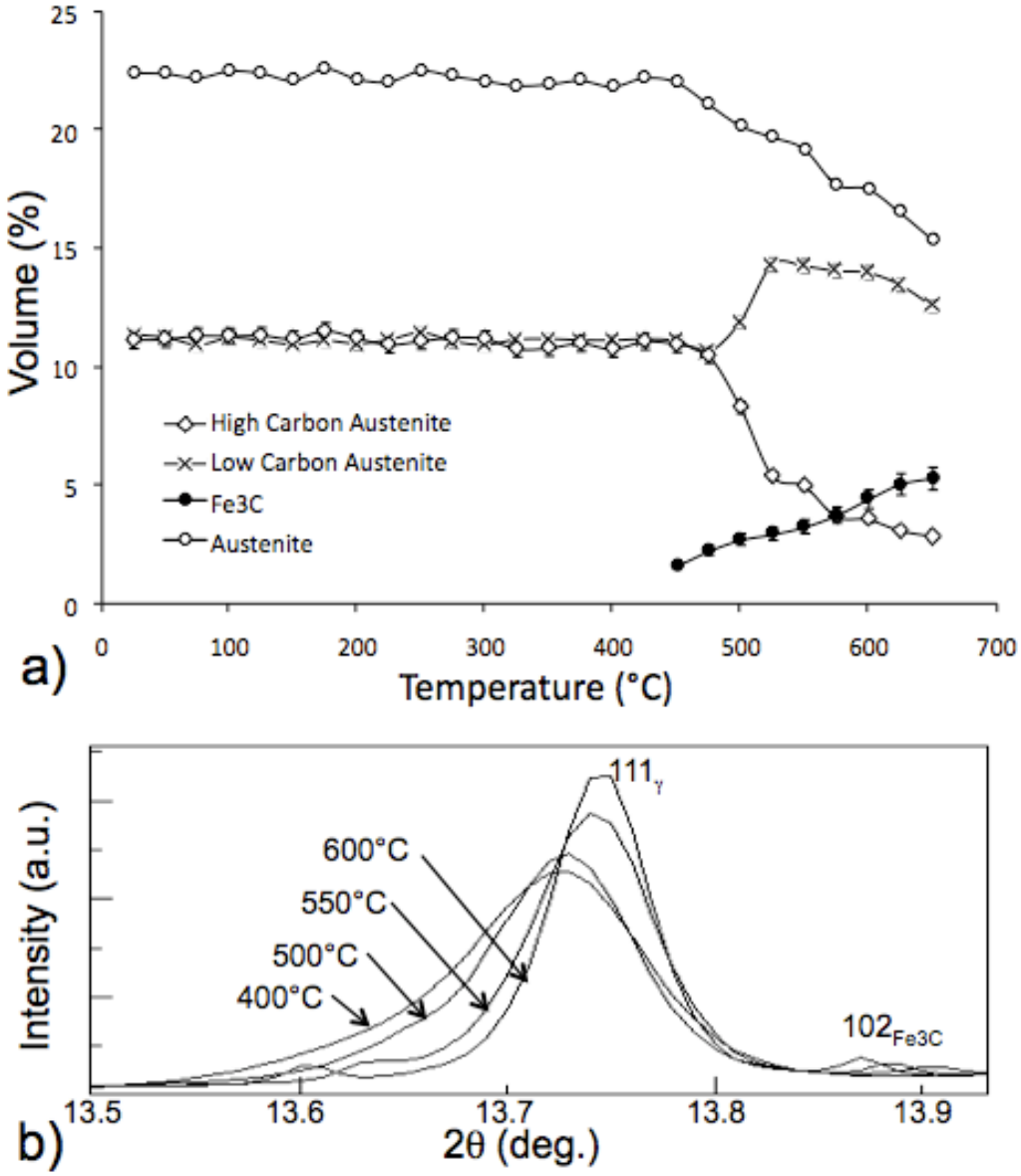

Fig. 11. Quantitative evolution of retained austenite and cementite during heat treatment (a). The 111 austenite peak profile changes during heating is also shown (b).

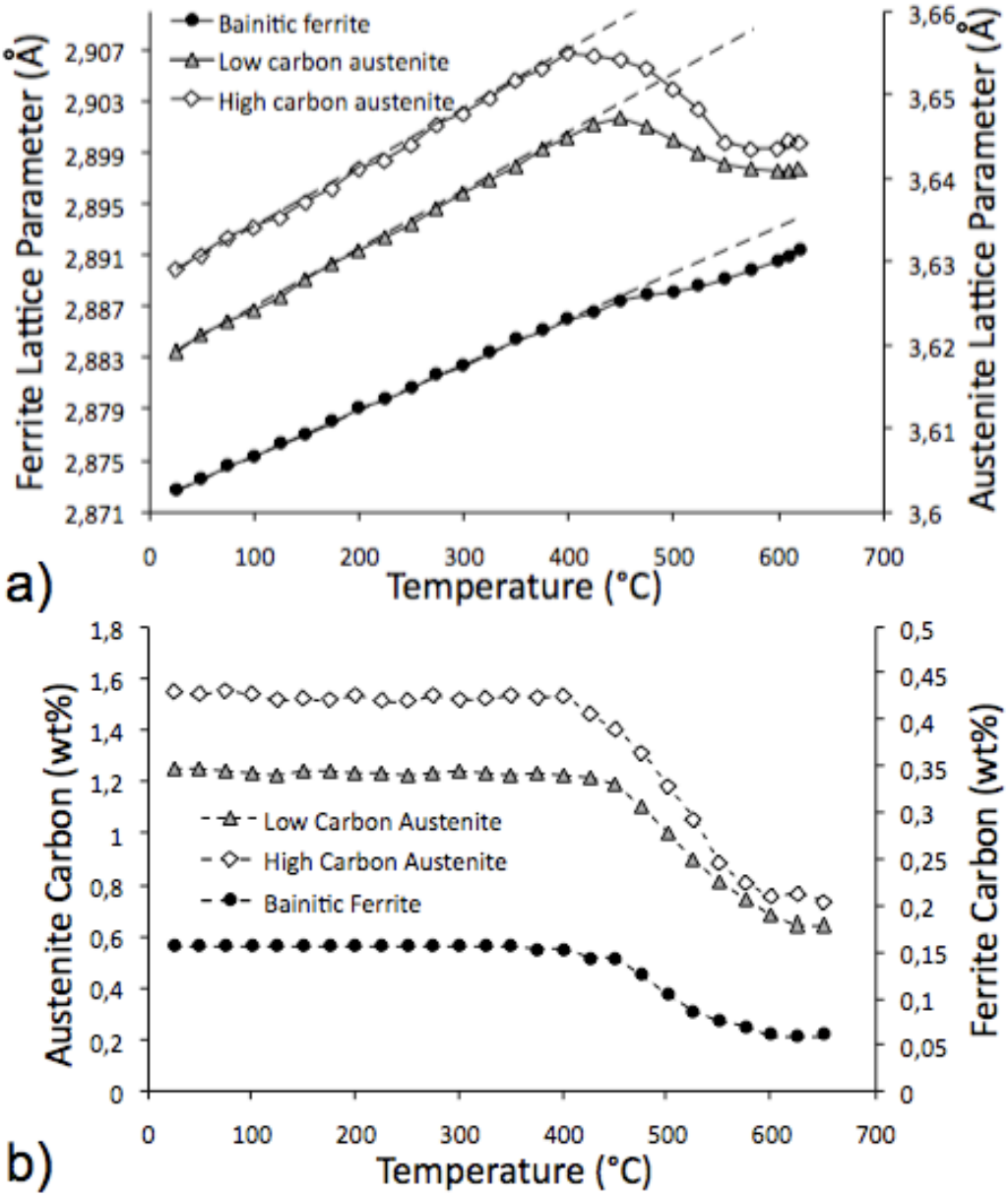

Fig.12. Lattice parameter of austenite and bainitic ferrite as a function of temperature (a). The evolution of carbon content with the temperature is shown in (b).

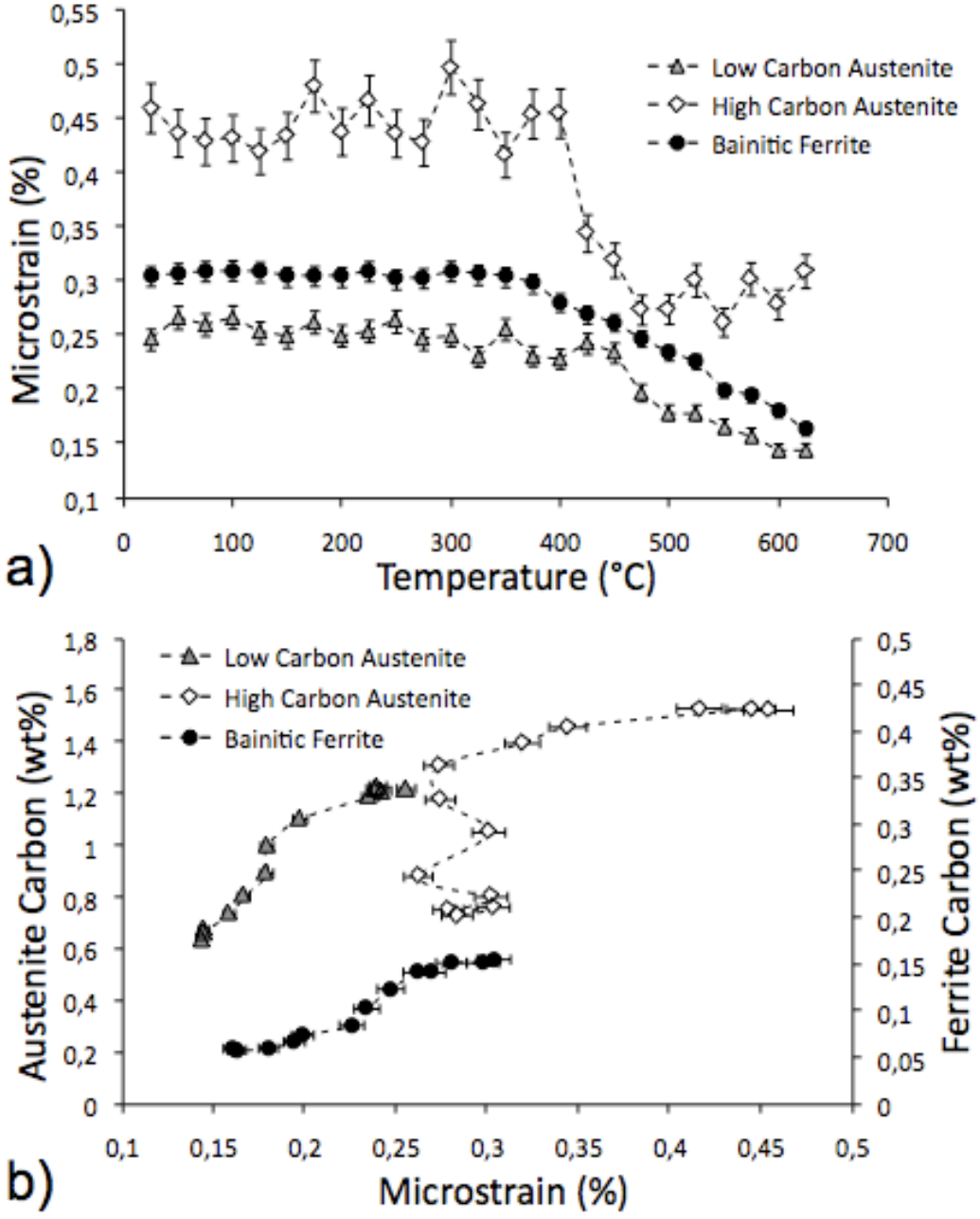

Fig.13. Microstrain evolution as a function of temperature (a), and austenite and ferrite carbon concentration as a function of microstrain (b).